Rolled-Up Optical Microcavities with Subwavelength Wall Thicknesses for Enhanced Liquid Sensing Applications

Gaoshan Huang,[†,*] Vladimir A. Bolaños Quiñones,[†] Fei Ding,[†] Suwit Kiravittaya,[†] Yongfeng Mei,[†,‡,*] and Oliver G. Schmidt[†]

[†]Institute for Integrative Nanosciences, IFW Dresden, Helmholtzstr. 20, D-01069 Dresden, Germany, and [‡]Department of Materials Science, Fudan University, Shanghai, 200433, Peoples's Republic of China

ABSTRACT Microtubular optical microcavities from rolled-up ring resonators with subwavelength wall thicknesses have been fabricated by releasing prestressed SiO/SiO_2 bilayer nanomembranes from photoresist sacrificial layers. Whispering gallery modes are observed in the photoluminescence spectra from the rolled-up nanomembranes, and their spectral peak positions shift significantly when measurements are carried out in different surrounding liquids, thus indicating excellent sensing functionality of these optofluidic microcavities. Analytical calculations as well as finite-difference time-domain simulations are performed to investigate the light confinement in the optical microcavities numerically and to describe the experimental mode shifts very well. A maximum sensitivity of 425 nm/refractive index unit is achieved for the microtube ring resonators, which is caused by the pronounced propagation of the evanescent field in the surrounding media due to the subwavelength wall thickness design of the microcavity. Our optofluidic sensors show high potential for lab-on-a-chip applications, such as real-time bioanalytic systems.

KEYWORDS: nanomembrane · sensor · microcavity · rolled-up nanotech · lab-on-a-chip

In recent years, optical ring resonators, used to filter and confine light at certain resonant wavelengths in small volumes, have gained considerable interest both for practical applications and for fundamental scientific research.[1−10] Especially, design and fabrication of novel label-free optical sensors based on ring resonators, which can be employed to measure the physical, chemical, and biological properties of surrounding materials is attracting increasing attention.[11−19] Compared to other label-free optical sensors such as surface plasmon resonance instruments and interferometers,[20,21] microtubular optical ring resonators, operated as optofluidic components, have already shown the possibility for successful integration of ring resonators and microfluidics[22] and thus promise high potential for lab-on-a-chip applications.

In optical ring resonators, the whispering gallery modes (WGMs) form due to total internal reflection of light at the boundary between the high and low refractive index media.[17] However, the light energy cannot be completely confined in the resonator wall of high refractive index medium. The evanescent field penetrates into the low refractive index medium and interacts with the materials near the interface, leading to a wavelength shift of the light circulating in the optical ring resonator. Thus, sensing applications of ring resonators are realized by simply detecting spectral shifts of the optical resonant modes.[17,22] Previous investigations have demonstrated that the sensitivity of those sensors depends on the energy of the light propagating in the low refractive index medium.[17,18] In order to increase the sensitivity of the optical sensor, it is necessary to reduce the thickness of the high refractive index medium (*i.e.*, wall thickness of the resonator), which reduces the light confinement in the resonator and correspondingly increases the intensity of the evanescent field in the surrounding medium. Unfortunately, previous optical sensors derived from glass capillaries experience outer radii of 35−50 μm and wall thicknesses of 2−4 μm,[22,23] leading to low sensitivities of less than 35 nm/refractive index unit (RIU).[11,12,17] The large size of the sensors also renders large-scale integration for on-chip applications difficult and requires abundant consumption of test media. We believe that these shortcomings for glass capillaries can be successfully overcome by a newly developed rolled-up nanotechnology.[24−28] This technology involves growing a prestressed nanomembrane on a sacrificial layer and then etching away the underneath sacrificial layer to release the prestressed nanomembrane, which rolls up into a microtubular structure. Employing this general strategy, we are able to fabricate optical microcavities (*i.e.*, optical ring resonators) with defined

*Address correspondence to gaoshan.huang@gmail.com, y.mei@ifw-dresden.de.

Received for review March 5, 2010 and accepted May 24, 2010.

Published online June 7, 2010.
10.1021/nn100456r

diameters and subwavelength wall thicknesses.[29,30] The refractive index of the microcavity wall can be easily tuned by rolling up different materials or material combinations or simply by performing several rotations.[4,5,31−37] The demonstration of rolled-up nanomembranes as transparent cell culture scaffolds emphasizes the promising future of rolled-up microcavities in bioapplications such as real-time cell detection.[38]

In this work, we have successfully fabricated microcavities from rolled-up nanomembranes with subwavelength wall thickness. The optical modes supported in the microcavities are measured by means of photoluminescence (PL), and pronounced spectral shifts of the mode positions are observed from the optical microcavity in different surrounding media. Good agreement is found between experimental results and analytical calculations as well as simulations using the finite-difference time-domain (FDTD) method. A maximum sensitivity of 425 nm/RIU is achieved, which is much higher than what has been reported in glass capillary sensors.[11,12,17] However, due to the smaller quality factor of our rolled-up microcavities, the detection limit is around 10^{-4} RIU, hindering the device from sensing tiny changes of refractive index, which could be further improved by structure optimization. For sensing large changes of refractive index, the high sensitivity of our rolled-up microcavities is beneficial, providing a cheap and simple way to produce large spectral shifts for detection.

RESULTS AND DISCUSSION

Figure 1a displays a three-dimensional schematic diagram of a rolled-up SiO/SiO_2 nanomembrane with additional oxide coating layers on both inner and outer surfaces immersed in liquid. The top-left inset shows an optical microscope image of an ordered array of rolled-up microtubular structures on a Si substrate. All of the rolled-up nanomembranes are aligned into the same direction due to the applied glancing angle deposition technique (see Methods). The bottom-left inset shows a bird's-eye view SEM image of the opening of a rolled-up nanomembrane, demonstrating a perfectly circular shape. The microtubes have a uniform diameter (d) of 7.5 μm and are rolled-up from square-shaped nanomembranes with a side length of $D = 70$ μm. The number of rotations (N) is given by $N = D/(\pi d)$ and equals ~3 rotations in the present case. The quality and dimension (*e.g.*, diameter and the number of rotations) of the rolled-up nanomembranes are directly determined by the stain gradient generated during thin-film deposition. For instance, the diameter of the rolled-up microtubes increases almost linearly with total thickness of the SiO/SiO_2 bilayer.[10] Here, we use a bilayer thickness of less than 40 nm, and the corresponding diameter is less than 10 μm. The thickness ratio between the SiO and SiO_2 layers is another important parameter to obtain tightly rolled-up nanomembranes. In our experiment, several thickness ratios were tested and a value of ~1:4 was found to be particularly well-suited for the roll-up process. In addition, since the nanomembranes are predefined by photolithography, we can easily tune the resonant modes by adjusting the shape of the microcavity. We have already demonstrated that the optical modes shift along the axis of a microtube rolled-up from a circular nanomembrane.[9] Here, we focus on rolled-up nanomembranes formed from square patterns because of a uniform wall thickness along the tube axis and therefore spatially constant mode energies.[9] The roll-up process allows for accurate positioning of microtubes on a substrate and renders large-scale integration of such devices feasible for future on-chip applications.

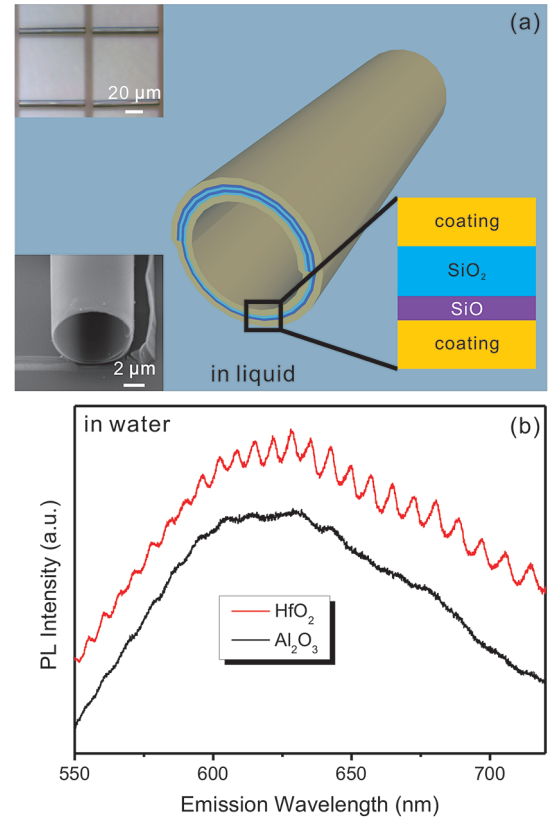

Figure 1. (a) Three-dimensional schematic diagram of a rolled-up nanomembrane in liquid. The bottom-right inset illustrates the multilayer structure of the wall; the top-left inset shows an optical microscope image of an ordered array of rolled-up nanomembranes; and the bottom-left inset shows a bird's-eye view SEM image of the opening of a rolled-up nanomembrane. (b) PL spectra obtained in water from rolled-up nanomembranes with HfO_2 and Al_2O_3 coating layers (30 nm thick for both cases), taken under excitation of the 442 nm line of a He−Cd laser.

Figure 1b shows PL spectra from two rolled-up nanomembranes in water, one coated with Al_2O_3, the other with HfO_2. In both spectra, a broad light emission band is observed (excitation: 442 nm line of He−Cd laser), which is assigned to defect-related emission centers on the surface of Si clusters in the SiO/SiO_2 film.[9,39,40]

A modulation in PL intensity is observed (especially in the spectrum from the HfO_2-coated microtube), which is assigned to WGMs[32,34,35] in this special type of optical ring resonator/microcavity.[32] However, the quality factor and the intensity of the WGMs is quite low compared to those in optical resonators made from glass capillaries.[9,17,22] The difference is mainly due to the light loss induced by the very thin wall of the rolled-up optical microcavity, which is normally less than 200 nm (subwavelength) thick (compared to 2−4 μm wall thickness in glass capillary resonators).[22,23] A wall thickness smaller than the light wavelength reduces the light confinement, leading to pronounced light diffraction and evanescent field propagation into the surrounding low refractive index medium. The strong light loss reduces the photon lifetimes and broadens the modes, resulting in low relative intensities and quality factors.[32] We stress, though, that the strong loss of the light is not necessarily a limitation for sensing applications but instead can even enhance the sensitivity of the device.[17,18] Nevertheless, huge loss of light leads to a considerable degradation of the quality factor of the mode and even renders the modes from rolled-up nanomembranes undetectable. Although the evanescent field in the surrounding medium is enhanced, the detection limit is sacrificed due to low quality factors of the modes. Therefore, atomic layer deposition (ALD) to increase the wall thickness and refractive index is used in our experiment to achieve a balance between these two counteracting tendencies. As we can see in Figure 1b, the HfO_2 effectively improves the light confinement compared to the Al_2O_3 coating since HfO_2 has a larger refractive index. Here, we use a 30 nm HfO_2 coating layer to obtain acceptable mode intensities, detection limit (which will be discussed later), and high optical sensitivities, simultaneously. The combination of rolled-up nanotechnology and ALD post-treatment presented in this work demonstrates a flexible method to adjust the balance between detection limit and sensitivity required for many sensing applications.

For sensing applications, we measured the PL spectra of the rolled-up nanomembranes in different liquids. Figure 2 shows the spectra from a microcavity with a diameter of ~9 μm in air, deionized water, ethanol, and water/ethanol mixture (1:1 in volume). WGMs are observed in all four spectra, but striking differences are present. The spectrum from the microcavity in air reveals a double-peak structure, which is absent in the spectra from the microcavities in the liquids. In our previous work,[10] polarization-dependent PL measurements revealed two groups of modes, which were identified as transverse magnetic modes (TM modes, with electric field vector parallel to the tube axis) and transverse electric modes (TE modes, with magnetic field vector parallel to the tube axis). The TE modes only exist in microtube ring resonators with thick walls and therefore small diffraction loss.[10,32] When the optical microcavity

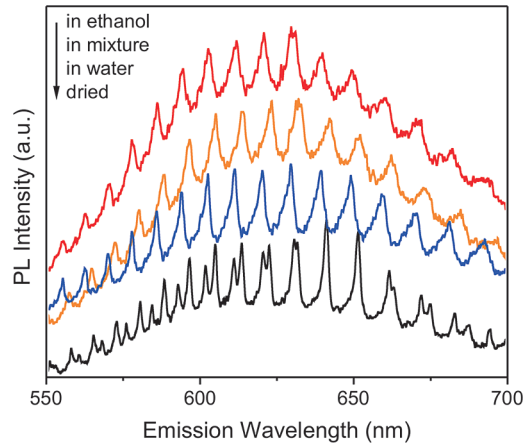

Figure 2. PL spectra of an optical microtube cavity with a diameter of ~9 μm in air, deionized water, ethanol, and water/ethanol mixture (1:1 in volume). All microcavities were excited by a frequency-doubled Nd:YVO_4 laser operated at 532 nm. The intensity of each spectrum is normalized to its strongest mode.

is immersed into the liquids, higher refractive indices of the surrounding liquids increase the light loss for both TM and TE modes. However, the loss for TE modes is much more prominent than for the TM modes, making the TE modes undetectable in the liquids. Two-dimensional FDTD simulations (Lumerical Solutions software) were performed to obtain the intensity and electric/magnetic field patterns of the modes in the rolled-up nanomembranes. The film thicknesses and refractive indices used in the simulation are obtained from ellipsometry measurements, and the values of refractive indices are 1.55, 1.45, and 1.95 for SiO, SiO_2, and HfO_2 layers, respectively. The results derived from FDTD simulations are depicted in Figure 3. Figure 3a compares normalized intensities of the TM and TE modes. Both intensities of the TM and TE modes greatly decrease in water (n_{water} = 1.33) and ethanol ($n_{ethanol}$ = 1.36) due to diffraction loss, but the intensities of the TM modes remain about 1 order of magnitude higher than those of the TE modes. This phenomenon is further visualized by the field patterns displayed in Figure 3b. The four panels in Figure 3b display field (magnetic field for TE mode and electric field for TM mode) patterns for optical microcavities in different surrounding media. For air, both fields are well-confined to the wall. However, pronounced dissipation of the magnetic field in the water leads to the disappearance of the TE modes, which is consistent with our observations in Figure 3a.

In addition to the vanishing TE modes in liquids, another interesting phenomenon is observed. The WGMs in Figure 2 shift spectrally when the microcavity is immersed and measured in different liquids, implying an optofluidic sensing function of the rolled-up nanomembrane. However, due to the periodic peak structure of the modes, an unambiguous assignment of the mode shifts is difficult. An analytical calculation was therefore

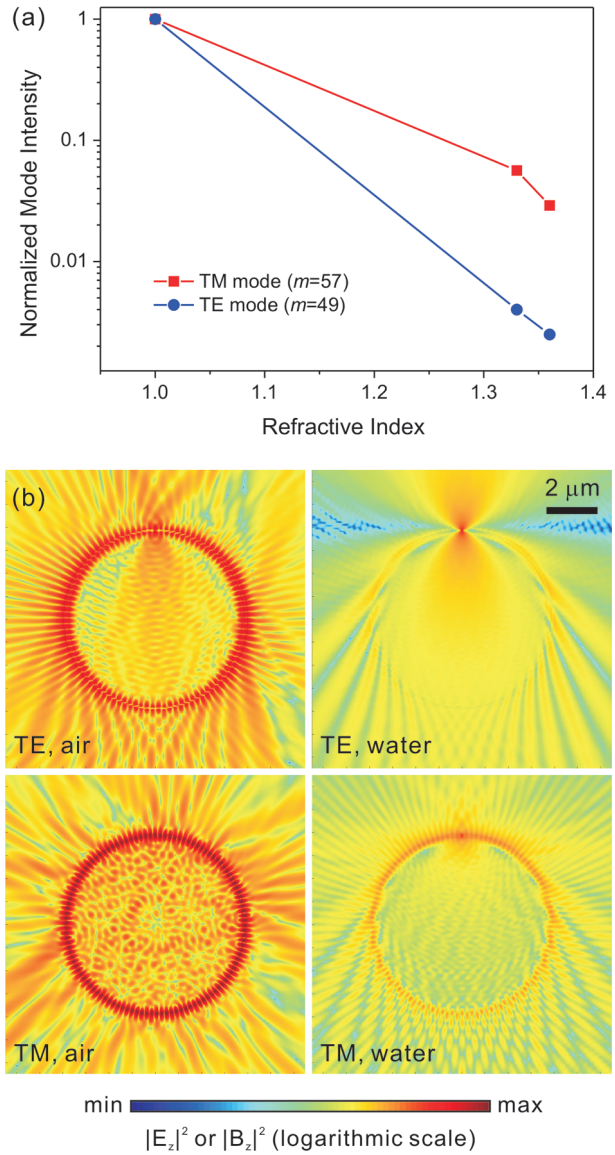

Figure 3. (a) Normalized TM and TE mode intensities as a function of refractive index of surrounding medium. (b) Simulated field patterns (magnetic field for TE mode and electric field for TM mode) of corresponding TE and TM modes for optical microcavity in different surrounding media. The intensities are displayed in logarithmic scale to elucidate the remarkable diffraction loss of the light.

carried out based on Maxwell equations applied to the geometric structure of the rolled-up nanomembrane (for more details, see Supporting Information). In our approach, only the cross section of the optical microcavity is considered, which leads to a solution in two dimensions. Another approximation is that the spiral structure is treated as a planar waveguide, ignoring the notches at the rolling edge of the nanomembrane and the curved surface of the microcavity.[32,34] The length of the equivalent planar waveguide is the circumference of the tube. Since, in general, the number of rotations is not an integer, the average thickness of the nanomembrane is taken and used as the height of the planar waveguide. In addition, the refractive index of the planar waveguide is obtained *via* averaging refractive indices of the layers in the microtube wall. By applying the correct boundary conditions, the Maxwell equations can be solved (see Supporting Information):[41]

$$\tan(\gamma h) = \frac{2\delta/\gamma}{1 - (\delta/\gamma)^2} \quad (1)$$

where $\delta^2 = (2m/d)^2 - (2n_2\pi/\lambda_0)^2$ and $\gamma^2 = (2n_1\pi/\lambda_0)^2 - (2m/d)^2$, λ_0 is the mode position, m is an integer (azimuthal number), and n_1 and n_2 are refractive indices of the microcavity wall and surrounding medium, respectively. Unfortunately, this transcendent eq 1 can only be solved numerically. The calculated mode positions as a function of azimuthal number and refractive index of the surrounding medium for an optical microcavity with a diameter of ~9 μm are displayed in Figure 4 (note that the azimuthal numbers should be discontinuous integers indicated by solid lines). For a certain azimuthal number, pronounced optical shifts of the WGMs to longer wavelengths are observed when the refractive index is increased from 1 to 1.38 and a maximum shift of more than 90 nm for $m = 48$ is determined. For comparison, we also carried out two-dimensional FDTD simulations with the same parameters used in the analytical calculation but including the spiral structure and curvature of the wall. The FDTD simulations show the same tendency for the mode shifts and also agree well with our experimental results (see Table S2, Supporting Information). Although several approximations are made in our analytical approach, results with good veracity are obtained with much shorter computing time compared to FDTD simulations. We therefore conclude that the analytic method is applicable for fast characterization of a rolled-up optical microcavity.

To check the sensing function of our optical microcavities in different liquids, we measured PL spectra from a rolled-up nanomembrane ($d \sim 7$ μm) in air, deionized water, and isopropyl alcohol. Features similar to those shown in Figure 2 are observed, indicating quite generally that the optical microcavities are useful in applications such as sensing refractive indices of different liquids. To explore the sensing performance of the microcavities in more detail, we plot the mode positions in Figure 5 and add the simulated mode positions (calculated by FDTD) as solid lines for comparison. From this diagram, we can easily correlate the modes from the microcavity in different liquids. The slopes of the solid lines increase for higher refractive indices, suggesting a higher sensitivity in liquids with higher refractive index.

On the basis of the FDTD simulations and the experimental data for water and isopropyl alcohol/ethanol, we determine the sensitivity S of the rolled-up optical microcavity at the refractive index 1.33 of water by

$$S = \frac{\lambda_{m,liquid} - \lambda_{m,water}}{n_{liquid} - n_{water}} \quad (2)$$

where $\lambda_{m,liquid}$ ($\lambda_{m,water}$) represents the mode position of TM modes in liquid (water) with the same azimuthal number m, and n_{liquid} (n_{water}) denotes the corresponding refractive index of the liquid (water). Experimental results from two optical microcavities are given in Figure 6 as black squares. Figure 6a shows the sensitivity of a big microcavity ($d \sim 9$ μm) by applying eq 2 to ethanol and water, while Figure 6b displays the results for a small microcavity ($d \sim 7$ μm) which was immersed in isopropyl alcohol and water. The sensitivities for both optical microcavities are substantially higher than those reported previously.[11,12,17] It is worth noting that, due to slight variations in the fabrication process, the sensitivity of the large microcavity in Figure 6a is slightly higher than that of the small microcavity in Figure 6b. To understand the mechanism in more detail, we calculated the quality factors of the microcavities. The quality factors of the big microcavity in air and liquid are ~480 and ~220, respectively, for the mode at ~2 eV, and those of the small microcavity are ~660 and ~250, respectively. Since the quality factor of the microcavity is determined by the energy loss, we may infer that the energy loss in the big microcavity is higher than that in the small microcavity. A large part of the evanescent field penetrates into the surrounding medium so that the change in refractive index of the medium has a large influence on the light propagation in the microcavity.[17,18] As a consequence, the sensitivity of the big microcavity increases. Apart from the sensitivity, the detection limit (DL) is another important parameter for optical sensors. Here, the detection limit of our microcavities is calculated by

$$\mathrm{DL} = 3\sigma/S \qquad (3)$$

where σ is the standard deviation of the system noise/spectral resolution and S the sensitivity;[12] σ is determined by the line width of the mode and the thermal noise. According to our PL spectra, the line width of the mode at ~2 eV is around 3 nm for both microcavities, and therefore, the weak thermal noise is omitted in this estimation.[12] Similar to previous calculations,[12,42] 1/50 of the line width can easily be resolved and are used as σ. Thus, the obtained detection limit of our microcavities is in the order of 10^{-4} RIU. Due to the lower quality factor, the detection limit of rolled-up microcavities presented here is larger than that of glass capillaries,[11,12] indicating that presently our microcavities can hardly be used to sense tiny fluctuations in refractive index produced by trace solutions. However, considering that the sensitivity and detection limit can be effectively tuned by ALD coating, we believe that the rolled-up microcavities can easily find beneficial use in analytical chemistry and bioanalytic systems.

Another notable phenomenon in Figure 6 is the decrease of the sensitivity with increasing azimuthal number (see red dashed lines in Figure 6a,b), which is considered to be due to stronger light confinement in the

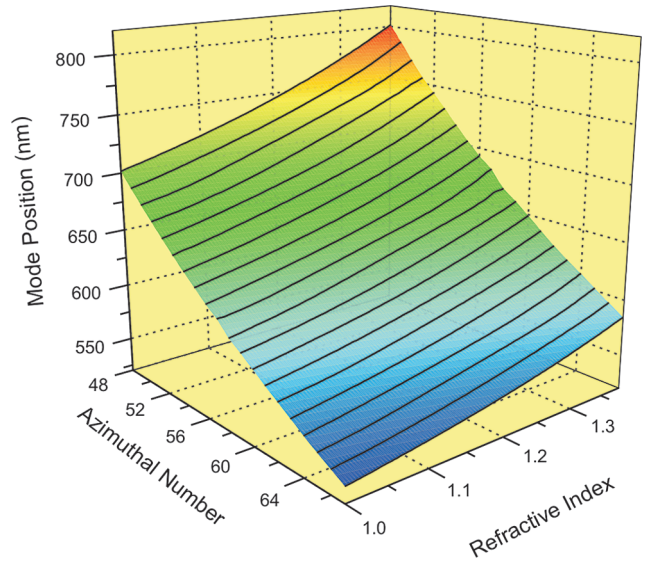

Figure 4. TM mode position from an optical microcavity with a diameter of ~9 μm as a function of azimuthal number and refractive index of surrounding medium. The mode shifts with different azimuthal numbers are derived from calculations (see Supporting Information).

microtube wall. Since the azimuthal number denotes the number of the nodes of the field intensity around the ring, a larger azimuthal number corresponds to more nodes in the microcavity, which effectively enhances the field confinement in the optical microcavity. As one can see in Figure 6c, the diffraction loss is much more prominent in the field pattern of the mode with lower azimuthal number (left panel). Hence, we may further improve the sensitivity by operating the sensors in a longer wavelength range (*i.e.*, smaller azimuthal number), which, however, would lead to even lower quality factor and larger detection limit.

So far, our experimental results demonstrated that, in principle, the rolled-up nanomembranes can be used

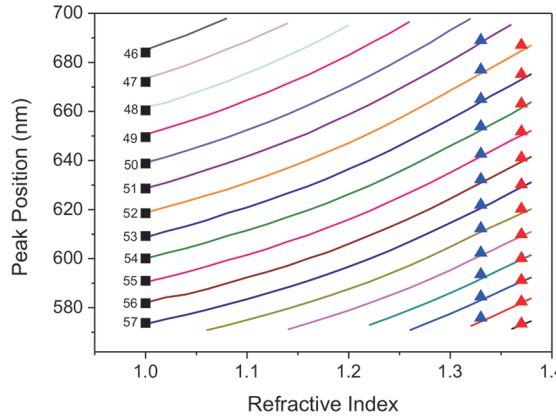

Figure 5. Mode position of TM mode from an optical microcavity with a diameter of ~7 μm as a function of refractive index of surrounding medium. The solid lines are derived from FDTD simulations, and the black squares, blue triangles, and red triangles represent experimental mode positions in air, deionized water, and isopropyl alcohol, respectively. The corresponding azimuthal numbers are also indicated.

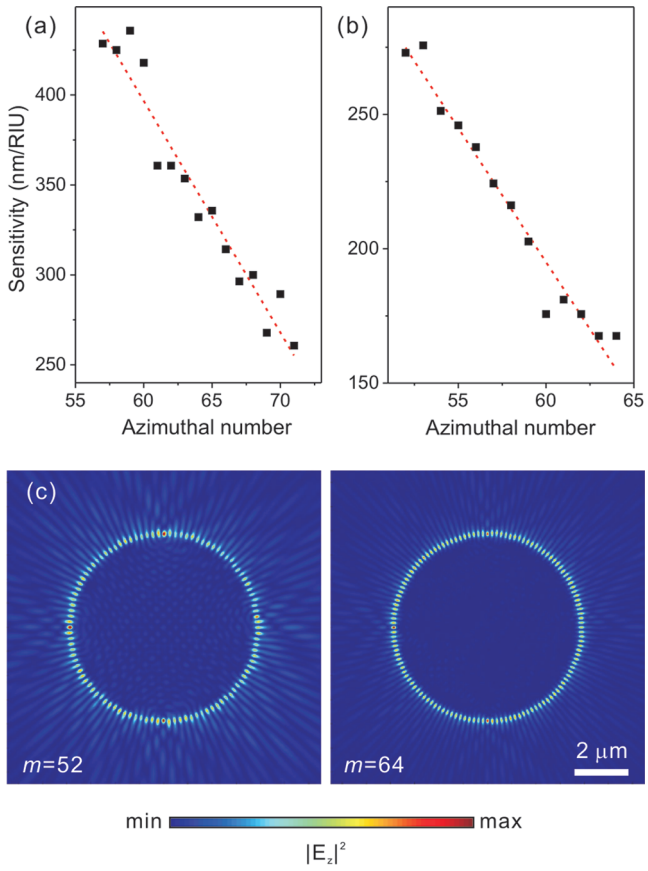

Figure 6. Sensitivity as a function of azimuthal number, obtained from an optical microcavity with a diameter of (a) ~9 μm and (b) ~7 μm. (c) Simulated electric field patterns of TM modes with different azimuthal numbers for an optical microcavity with a diameter of ~7 μm in water. The intensities are displayed in linear scale to illustrate the light confinement in the tube wall.

as optical microcavities and optical sensor prototypes with enhanced sensitivity. To realize real-time sensing of the refractive index change of the flowing liquid inside rolled-up microtubes with femtoliter volumes, we need to fabricate microtube-based optofluidic devices. This is certainly feasible because the roll-up microcavities are fabricated with the aid of photolithography and the device can easily be produced and integrated by straightforward pattern design.[30] In the integrated device, the sensitivity and the detection limit are tuned by structural design and the rolled-up nanomembranes are used as fluidic channels and optical microcavities simultaneously, forming liquid core optical resonators.[12,23] We also propose to improve the optical measurements by engaging an optical fiber taper which is in contact with the rolled-up nanomembrane. When the wavelength of the light meets the resonant condition of the optical microcavity, the light can be coupled into the microcavity, leading to reduction in output power.[12,22,43] This can easily be measured to precisely determine the position of WGM. Further work concerning the production of this real-time optofluidic sensor device is currently in progress in our group.

CONCLUSIONS

We have successfully fabricated optical microcavities with subwavelength wall thickness from rolled-up nanomembranes. The geometrical structure and the position of the microcavities on the substrate can be precisely controlled by conventional photolithography. Excellent sensing functionality is demonstrated by pronounced spectral shifts of the WGMs immersed in liquids. Mode shifts to longer wavelength with increasing refractive index of the surrounding medium are well-described by analytical calculations, and the experimental data can be well-fitted by FDTD simulations. On the basis of the simulations, we can unambiguously assign the modes and determine the sensitivity of the sensor. The highest sensitivity measured in our experiment reaches 425 nm/RIU, which is higher than previous results obtained from glass capillaries. Very thin microtube walls are the origin of the high sensitivity and could be further optimized by adjusting their thickness by ALD. However, the substantial light loss due to the thin wall also deteriorates the quality factor of the microcavity, resulting in a relatively large detection limit, which could be improved by further optimization of the microcavity structure. We expect that this kind of rolled-up optical sensor can be easily integrated into a bioanalytic tubular microchannel for lab-on-a-chip applications. For instance, a multifunctional lab-in-a-tube may be fabricated in this way to detect and analyze individual cells, biomolecules, and their bioactivities.

METHODS

Rolled-Up Nanomembrane: A uniform ARP-3510 photoresist (Allresist GmbH) layer was deposited on a Si(100) wafer by spin-coating at a speed of 3500 rotations per minute. This ~2 μm thick photoresist layer was patterned into square shape with different sizes by using conventional photolithography technology and was used as a sacrificial layer in the roll-up process. The active layer (SiO/SiO_2 bilayer structure) was deposited under high vacuum ($<10^{-4}$ Pa) by electron beam evaporation with a glancing angle of 60°, which produces a gap at the far end of the photoresist pattern due to the ballistic shadow effect.[18] The film thickness is *in situ* monitored by a quartz crystal deposition controller and double-checked by ellipsometry measurement after deposition. A thickness ratio of ~1:4 between SiO and SiO_2 is found to be the optimal parameter for the roll-up process. To obtain rolled-up optical microcavities with different dimensions (*e.g.*, diameter and the number of rotations), different bilayer thicknesses and pattern sizes were adopted in our experiments. The underetching was conducted by putting the samples in the chamber of a critical point dryer (CPD030, Bal-Tec AG), which was filled with acetone (BASF GmbH). The acetone penetrated through the gap and removed the photoresist layer, releasing the SiO/SiO_2 layer. The intrinsic stress in the SiO/SiO_2 bilayer structure made the free-standing films bend up and self-assemble into a microtubular structure. The rolled-up nanomembranes were then dried in the critical point dryer by using liquid CO_2 as intermedia to avoid the collapse of the rolled-up structures. After the formation of the rolled-up nanomembrane,

an Al_2O_3 or HfO_2 layer was deposited onto both the inner and outer surfaces of the rolled-up nanomembranes by ALD (Savannah 100, Cambridge NanoTech Inc.) to strengthen the optical microcavities mechanically and also improve intensity of optical modes. The oxide layers were deposited under optimized conditions: Al_2O_3 layers were deposited at 80 °C (0.9 Å per cycle), while the HfO_2 layers were deposited at 130 °C (1 Å per cycle).

Microscopy: The morphologies of rolled-up nanomembranes were checked using scanning electron microscopy (SEM, in Zeiss NVision40 workstation) and optical microscopy (Zeiss Axiotech vario) connected to a camera (Zeiss AxioCam MR) for high-resolution color images.

PL Measurements: The optical properties of rolled-up nanomembranes were characterized by micro-PL spectroscopy at room temperature with excitation lines at 532 nm (frequency-doubled Nd:YVO_4 laser) and 442 nm (He−Cd laser in a Renishaw inVia micro-Raman system) at room temperature. The emission spectra were collected *via* a 20× long-working-distance objective. For the sensing application experiments, the substrate with rolled-up nanomembranes was fixed using double-side tape in a Petri dish placed on the stage of the microscope. Different liquids (deionized water, isopropyl alcohol (BASF GmbH), ethanol (BASF GmbH), and mixed solution) were poured gently into the Petri dish until the rolled-up nanomembranes were completely immersed and the microcavities were fully filled. The liquid was removed carefully using pipettes after each measurement. The microscope image was monitored during the whole measurement to ensure the emission signal is collected from exactly the same position of the microcavity.

Acknowledgment. We are grateful for experimental help by J. D. Plumhof, P. Cendula, Dr. L. B. Ma, Dr. A. Rastelli, Dr. M. Benyoucef, Dr. I. Mönch, B. Eichler, R. Engelhard, E. J. Smith, Dr. H. S. Lee, S. Kumar, and Dr. J. S. Becker. This work was financially supported by the Grants from the Volkswagen Foundation (I/84 072) and a Multidisciplinary University Research Initiative (MURI) sponsored by the U.S. Air Force Office of Scientific Research (AFOSR) Grant No. FA9550-09-1-0550.

Supporting Information Available: Analytical calculation of WGMs based on Maxwell equations. This material is available free of charge *via* the Internet at http://pubs.acs.org.

REFERENCES AND NOTES

1. Armani, D. K.; Kippenberg, T. J.; Spillane, S. M.; Vahala, K. J. Ultra-high-Q Toroid Microcavity on a Chip. *Nature* **2003**, *421*, 925–928.
2. Vahala, K. J. Optical Microcavities. *Nature* **2003**, *424*, 839–846.
3. Ksendzov, A.; Lin, Y. Integrated Optics Ring-Resonator Sensors for Protein Detection. *Opt. Lett.* **2005**, *30*, 3344–3346.
4. De Cort, W.; Beeckman, J.; James, R.; Fernández, F. A.; Baets, R.; Nezts, K. Tuning of Silicon-on-Insulator Ring Resonators with Liquid Crystal Cladding Using the Longitudinal Field Component. *Opt. Lett.* **2009**, *34*, 2054–2056.
5. Wu, X.; Sun, Y.; Suter, J. D.; Fan, X. Single Mode Coupled Optofluidic Ring Resonator Dye Lasers. *Appl. Phys. Lett.* **2009**, *94*, 241109.
6. Gondarenko, A.; Levy, J. S.; Lipson, M. High Confinement Micron-Scale Silicon Nitride High Q Ring Resonator. *Opt. Express* **2009**, *17*, 11366–11370.
7. Nitkowski, A.; Chen, L.; Lipson, M. Cavity-Enhanced On-Chip Absorption Spectroscopy Using Microring Resonators. *Opt. Express* **2008**, *16*, 11930–11936.
8. Bianucci, P.; Rodríguez, J. R.; Clements, C. M.; Veinot, J. G. C.; Meldrum, A. Silicon Nanocrystal Luminescence Coupled to Whispering Gallery Modes in Optical Fibers. *J. Appl. Phys.* **2009**, *105*, 023108.
9. Huang, G. S.; Kiravittaya, S.; Bolaños Quiñones, V. A.; Ding, F.; Benyoucef, M.; Rastelli, A.; Mei, Y. F.; Schmidt, O. G. Optical Properties of Rolled-Up Tubular Microcavities from Shaped Nanomembranes. *Appl. Phys. Lett.* **2009**, *94*, 141901.
10. Bolaños Quiñones, V. A.; Huang, G. S.; Plumhof, J. D.; Kiravittaya, S.; Rastelli, A.; Mei, Y. F.; Schmidt, O. G. Optical Resonance Tuning and Polarization of Thin-Walled Tubular Microcavities. *Opt. Lett.* **2009**, *34*, 2345–2347.
11. Yang, G.; White, I. M.; Fan, X. An Opto-fluidic Ring Resonator Biosensor for the Detection of Organophosphorus Pesticides. *Sens. Actuators, B* **2008**, *133*, 105–112.
12. Zhu, H.; White, I. M.; Suter, J. D.; Zourob, M.; Fan, X. Integrated Refractive Index Optical Ring Resonator Detector for Capillary Electrophoresis. *Anal. Chem.* **2007**, *79*, 930–937.
13. Son, S.; Grover, W. H.; Burg, T. P.; Manalis, S. R. Suspended Microchannel Resonators for Ultralow Volume Universal Detection. *Anal. Chem.* **2008**, *80*, 4757–4760.
14. Jokerst, N.; Royal, M.; Palit, S.; Luan, L.; Dhar, S.; Tyler, T. Chip Scale Integrated Microresonator Sensing Systems. *J. Biophotonics* **2009**, *2*, 212–226.
15. Ling, T.; Guo, L. J. Analysis of the Sensing Properties of Silica Microtube Resonator Sensors. *J. Opt. Soc. Am. B* **2009**, *26*, 471–477.
16. White, I. M.; Oveys, H.; Fan, X.; Smith, T. L.; Zhang, J. Integrated Multiplexed Biosensors Based on Liquid Core Optical Ring Resonators and Antiresonant Reflecting Optical Waveguides. *Appl. Phys. Lett.* **2006**, *89*, 191106.
17. Zhu, H.; White, I. M.; Suter, J. D.; Dale, P. S.; Fan, X. Analysis of Biomolecule Detection with Optofluidic Ring Resonator Sensors. *Opt. Express* **2007**, *15*, 9139–9146.
18. Sumetsky, M.; Windeler, R. S.; Dulashko, Y.; Fan, X. Optical Liquid Ring Resonator Sensor. *Opt. Express* **2007**, *15*, 14376–14381.
19. Monat, C.; Domachuk, P.; Eggleton, B. J. Integrated Optofluidics: A New River of Light. *Nat. Photonics* **2007**, *1*, 106–114.
20. Homola, J. Surface Plasmon Resonance Sensors for Detection of Chemical and Biological Species. *Chem. Rev.* **2008**, *108*, 462–493.
21. Ymeti, A.; Greve, J.; Lambeck, P. V.; Wink, T.; van Höovell, S. W. F. M.; Beumer, T. A. M.; Wijin, R. R.; Heideman, R. G.; Subramaniam, V.; Kanger, J. S. Fast, Ultrasensitive Virus Detection Using a Young Interferometer Sensor. *Nano Lett.* **2007**, *7*, 394–397.
22. Zhu, H.; White, I. M.; Suter, J. D.; Fan, X. Phage-Based Label-Free Biomolecule Detection in an Opto-fluidic Ring Resonator. *Biosens. Bioelectron.* **2008**, *24*, 461–466.
23. White, I. M.; Oveys, H.; Fan, X. Liquid-Core Optical Ring-Resonator Sensors. *Opt. Lett.* **2006**, *31*, 1319–1321.
24. Prinz, V. Ya.; Seleznev, V. A.; Gutakovsky, A. K.; Chehovskiy, A. V.; Preobrazhenskii, V. V.; Putyato, M. A.; Gavrilova, T. A. Free-Standing and Overgrown InGaAs/GaAs Nanotubes, Nanohelices and Their Arrays. *Physica E* **2000**, *6*, 828–831.
25. Schmidt, O. G.; Eberl, K. Nanotechnology—Thin Solid Films Roll up into Nanotubes. *Nature* **2001**, *410*, 168.
26. Mei, Y. F.; Huang, G. S.; Solovev, A. A.; Bermúdez Ureña, E.; Mönch, I.; Ding, F.; Reindl, T.; Fu, R. K. Y.; Chu, P. K.; Schmidt, O. G. Versatile Approach for Integrative and Functionalized Tubes by Strain Engineering of Nanomembranes on Polymers. *Adv. Mater.* **2008**, *20*, 4085–4090.
27. Solovev, A. A.; Mei, Y. F.; Bermúdez Ureña, E.; Huang, G. S.; Schmidt, O. G. Catalytic Microtubular Jet Engines Self-Propelled by Accumulated Gas Bubbles. *Small* **2009**, *5*, 1688–1692.
28. Mei, Y. F.; Thurmer, D. J.; Deneke, C; Kiravittaya, S.; Chen, Y. F.; Dadgar, A.; Bertram, F.; Bastek, B.; Krost, A.; Christen, J.; *et al.* Fabrication, Self-Assembly, and Properties of Ultrathin AlN/GaN Porous Crystalline Nanomembranes: Tubes, Spirals, and Curved Sheets. *ACS Nano* **2009**, *3*, 1663–1668.
29. Cavallo, F.; Songmuang, R.; Ulrich, C.; Schmidt, O. G. Rolling up SiGe on Insulator. *Appl. Phys. Lett.* **2007**, *90*, 193120.
30. Thurmer, D. J.; Deneke, C.; Mei, Y. F.; Schmidt, O. G. Process Integration of Microtubes for Fluidic Applications. *Appl. Phys. Lett.* **2006**, *89*, 223507.

31. Bernardi, A.; Kiravittaya, S.; Rastelli, A.; Songmuang, R.; Thurmer, D. J.; Benyoucef, M.; Schmidt, O. G. On-Chip Si/SiO_x Microtube Refractometer. *Appl. Phys. Lett.* **2008**, *93*, 094106.
32. Kipp, T.; Welsch, H.; Strelow, Ch.; Heyn, Ch.; Heitmann, D. Optical Modes in Semiconductor Microtube Ring Resonators. *Phys. Rev. Lett.* **2006**, *96*, 077403.
33. Songmuang, R.; Rastelli, A.; Mendach, S.; Schmidt, O. G. SiO_x/Si Radial Superlattices and Microtube Optical Ring Resonators. *Appl. Phys. Lett.* **2007**, *90*, 091905.
34. Hosoda, M.; Shigaki, T. Degeneracy Breaking of Optical Resonance Modes in Rolled-Up Spiral Microtubes. *Appl. Phys. Lett.* **2007**, *90*, 181107.
35. Strelow, Ch.; Rehberg, H.; Schultz, C. M.; Welsch, H.; Heyn, Ch.; Heitmann, D.; Kipp, T. Optical Microcavities Formed by Semiconductor Microtubes Using a Bottlelike Geometry. *Phys. Rev. Lett.* **2008**, *101*, 127403.
36. Mendach, S.; Songmuang, R.; Kiravittaya, S.; Rastelli, A.; Beyoucef, M.; Schmidt, O. G. Light Emission and Wave Guiding of Quantum Dots in a Tube. *Appl. Phys. Lett.* **2006**, *88*, 111120.
37. Strelow, Ch.; Schultz, C. M.; Rehberg, H.; Welsch, H.; Heyn, Ch.; Heitmann, D.; Kipp, T. Three Dimensionally Confined Optical Modes in Quantum-Well Microtube Ring Resonators. *Phys. Rev. B* **2007**, *76*, 045303.
38. Huang, G. S.; Mei, Y. F.; Thurmer, D. J.; Coric, E.; Schmidt, O. G. Rolled-Up Transparent Microtubes as Two-Dimensionally Confined Culture Scaffolds of Individual Yeast Cells. *Lab Chip* **2009**, *9*, 263–268.
39. Yi, L. X.; Heitmann, J.; Scholz, R.; Zacharias, M. Si Rings, Si Clusters, and Si Nanocrystals—Different States of Ultrathin SiO_x Layers. *Appl. Phys. Lett.* **2002**, *81*, 4248–4250.
40. Furukawa, K.; Liu, Y.; Nakashima, H.; Gao, D.; Uchino, K.; Muraoka, K.; Tsuzuki, H. Observation of Si Cluster Formation in SiO_2 Films through Annealing Process Using X-ray Photoelectron Spectroscopy and Infrared Techniques. *Appl. Phys. Lett.* **1998**, *72*, 725–727.
41. Marcuse, D. *Theory of Dielectric Optical Waveguides*, 2nd ed.; Academic Press: San Diego, CA, 1991; Chapter 1.
42. Arnold, S.; Khoshsima, M.; Teraoka, I.; Holler, S.; Vollmer, F. Shift of Whispering-Gallery Modes in Microspheres by Protein Adsorption. *Opt. Lett.* **2003**, *28*, 272–274.
43. Spillane, S. M.; Kippenberg, T. J.; Vahala, K. J. Ultralow-Threshold Raman Laser Using a Spherical Dielectric Microcavity. *Nature* **2002**, *415*, 621–623.